RESEARCH   **Open Access**

Quasi-linear analysis of dispersion relation preservation for nonlinear schemes

Fengyuan Xu, Pan Yan, Qin Li[*] and Yancheng You

*Correspondence:
qin-li@vip.tom.com;
q.li@xmu.edu.cn
School of Aerospace
Engineering, Xiamen
University, Xiang'an District,
Xiamen 361102, China

Abstract

In numerical simulations of complex flows with discontinuities, it is necessary to use nonlinear schemes. The spectrum of the scheme used has a significant impact on the resolution and stability of the computation. Based on the approximate dispersion relation method, we combine the corresponding spectral property with the dispersion relation preservation proposed by De and Eswaran (J Comput Phys 218:398–416, 2006) and propose a quasi-linear dispersion relation preservation (QL-GRP) analysis method, through which the group velocity of the nonlinear scheme can be determined. In particular, we derive the group velocity property when a high-order Runge–Kutta scheme is used and compare the performance of different time schemes with QL-GRP. The rationality of the QL-GRP method is verified by a numerical simulation and the discrete Fourier transform method. To further evaluate the performance of a nonlinear scheme in finding the group velocity, new hyperbolic equations are designed. The validity of QL-GRP and the group velocity preservation of several schemes are investigated using two examples of the equation for one-dimensional wave propagation and the new hyperbolic equations. The results show that the QL-GRP method integrated with high-order time schemes can determine the group velocity for nonlinear schemes and evaluate their performance reasonably and efficiently.

Keywords: Approximate dispersion relation, Dispersion relation preservation, Group velocity

1 Introduction

Nonlinear approaches, such as the weighted essentially non-oscillatory (WENO) scheme, are widely used to calculate complex flow fields with discontinuities, such as shock waves. Because of the mathematics of such schemes, truncation errors can affect the convergence rate of the computation and the spectral properties affect the deviation of the Fourier modes of the numerical results from the exact solution. Therefore, studying the spectral properties of nonlinear schemes is important and meaningful when developing high-order nonlinear schemes.

Tam and Webb [1] suggested that it was necessary to consider the spectral properties besides using the standard Taylor series method in the construction of difference schemes. Specifically, by using the Fourier transformation of the governing equation, they proposed a basic method for analyzing the dispersion and dissipation relation of a

linear scheme and developed a dispersion relation preservation (DRP) scheme. Moreover, this method can also be used to evaluate the spectral properties of different linear schemes and to construct new schemes. However, the method is inappropriate for analyzing the spectral properties of nonlinear schemes. To remedy this deficiency, Pirozzoli [2] studied the amplitude evolution of a disturbing mode after a tiny propagation period through a discrete Fourier transform (DFT), through which he proposed an approximate dispersion relation (ADR) analysis. ADR [2] gives an estimate of the total error generated by a nonlinear scheme and provides a method for analyzing its spectral properties. However, there are still some issues. For example, the time scheme can introduce errors, and if the grid number is not chosen carefully, there can be unexpected jumps in the spectral distribution [3].

Observing these problems, Mao et al. [3] proposed an improved ADR without time discretization called ADR-NT. Using the assumption of a tiny time period, they transferred the effect of the temporal derivative into the contribution of the spatial derivative. The researchers reported [3] that ADR-NT not only reduced the computational cost but also avoided the error due to the time discretization, as occurs in ADR. Mao et al. [3] also suggested ways to avoid jumping points when using ADR, i.e., the size of the grid should be twice some large prime or take the average over a large number of results with different initial phases.

The dispersion relation usually reflects the phase velocity of a spatial scheme. For practical problems with wave propagation, it is necessary to consider the group velocity, which is the one the energy propagates at [4]. De and Eswaran [5] analyzed the dispersion relation property of schemes from the perspective of the group velocity, which we refer to as the GRP method or just GRP. They pointed out that GRP was important when evaluating the spectral properties of linear schemes. In the space of the reduced wave number and frequency, group velocity preservation (GVP) occurs in the region where the ratio of the numerical group velocity to the theoretical group velocity is in [0.95, 1.05]. Obviously, the analyses of GRP proposed by De and Eswaran [5] are different from those of Tam and Webb [1] and Pirozzoli [2]. However, the GRP method can be used only for linear schemes and not for nonlinear schemes. Thus, we derived the modified wave number of nonlinear schemes with the ADR method, combined the aforementioned group velocity analysis with high-order Runge–Kutta schemes, and finally, derived a quasi-linear method to analyze the spectral properties of nonlinear schemes. For brevity, the method is called the QL-GRP method or just QL-GRP. Its rationality was then verified with a numerical test and the DFT method.

As usual, a one-dimensional wave propagation equation [5] is used in this study to explore the GVP of nonlinear schemes by QL-GRP. As shown in [5], for this governing equation, the group velocity is the same as the phase velocity. Therefore, it is insufficient to investigate the GVP of difference schemes. To overcome this, we devised hyperbolic equations such that the solutions are synthetic waves where the group velocity and phase velocity are different. Using the equations, we numerically analyzed the GVP of different difference schemes and also verified the validity of QL-GRP.

This paper is arranged as follows. The GRP and ADR methods are reviewed in Section 2. In Section 3, the GRP formula is derived for a high-order Runge–Kutta scheme, the QL-GRP method is described, and the comparative results from QL-GRP are given for typical schemes. In Section 4, the group velocities of selected cases are obtained

computationally using DFT and compared with those from QL-GRP, through which the rationality of QL-GRP is verified. We construct hyperbolic equations for which the solutions are waves where the group velocity and phase velocity are different. In Section 5, the one-dimensional wave propagation equation and the aforementioned hyperbolic equations are solved and analyzed. The conclusions are drawn in Section 6.

2 Review of GRP and ADR methods
Before we consider the QL-GRP method, the GRP and ADR methods are reviewed first.

2.1 GRP method
Consider the one-dimensional wave propagation equation [1–3, 5]:

$$u_t + cu_x = 0. \tag{1}$$

For the initial distribution $u(x,0) = \widehat{u}e^{ikx}$, Eq. (1) has the exact solution $u(x,t) = \widehat{u}e^{i(kx-\omega t)}$. For Eq. (1) it holds that $\omega = kc$. Therefore, the exact group velocity is $V_{g,exact} = d\omega/dk = c$.

When using a time scheme, the following approximate relation is obtained:

$$u(t_n + \Delta t) - u^n \approx u^{n+1} - u^n, \tag{2}$$

where u^n is the value at the initial time t_n, $u(t_n + \Delta t)$ is the exact solution at $t_n + \Delta t$, and u^{n+1} is the corresponding numerical solution. Suppose the variable distribution on t_n takes the form $u^n = \widehat{u}e^{i(kx-\omega t)}$. When the explicit Euler scheme is used for Eq. (1), Eq. (2) can be written as:

$$\widehat{u}e^{i[kx-\omega(t+\Delta t)]} - \widehat{u}e^{i(kx-\omega t)} \approx \Delta t \cdot f\left(t_n, u^n\right), \tag{3}$$

where $f(t_n, u^n)$ denotes the contributions from the spatial derivative. When a spatial scheme is used, one can see [5] that

$$f\left(t_n, u^n\right) = (-c)u_x = (-c)\frac{i\kappa'}{\Delta x}\widehat{u}e^{i(kx-\omega t)},$$

where κ' represents the modified wave number. It can be further derived from Eq. (3) that:

$$e^{-i\omega\Delta t} - 1 \approx \Delta t \cdot (-c) \cdot \frac{i\kappa'}{\Delta x}.$$

Following the approach of De and Eswaran [5], the numerical value $V_{g,num}$ of the Euler scheme can be derived by differentiating both sides of the above equation:

$$V_{g,num} = \left(\frac{d\omega}{dk}\right)_{num} = c\,\mathrm{Re}\left(e^{i\omega\Delta t} \cdot \frac{d\kappa'}{d\hat{\kappa}}\right) = c\left(\cos(\omega\Delta t)\frac{d\kappa_r'(\hat{\kappa})}{d\hat{\kappa}} - \sin(\omega\Delta t)\frac{d\kappa_i'(\hat{\kappa})}{d\hat{\kappa}}\right), \tag{4}$$

where $\omega\Delta t$ is the reduced frequency, $\hat{\kappa} = k\Delta x$ is the reduced wave number, and c is the theoretical group/phase velocity. Equation (4) is exactly the same as that proposed by De and Eswaran [5].

When a linear scheme is employed, the spatial derivative at x_i can be approximated by:

$$u_x(x_i) = \frac{1}{\Delta x} \sum_{j=-N}^{M} a_j u_{i+j},$$

where M and N are the numbers of nodes on the right and left sides of x_i, and a_j are the scheme coefficients. The modified wave number can be obtained by a Fourier transformation [1]:

$$\kappa'(\hat{\kappa}) = -i \sum_{j=-N}^{M} a_j e^{ij\hat{\kappa}}. \tag{5}$$

Once the dispersion and dissipation relations are obtained, $V_{g,\,num}$ for the first-order explicit Euler scheme can be obtained from Eq. (4). The explicit Euler scheme usually yields relatively large temporal errors, therefore the high-order Runge-Kutta schemes are employed in computations especially for unsteady problems. Hence, it is necessary to develop GRP analysis for high-order Runge-Kutta methods. Thus, Sengupta et al. [6] assumed that $a_4 + ib_4 = i\kappa'$ and $a_5 + ib_5 = \frac{d\kappa'}{d\hat{\kappa}}$, and derived the following GRP formula for the fourth-order Runge–Kutta scheme:

$$\frac{V_{g,num}}{c} = \frac{a_5 + 2\sigma(b_4 b_5 - a_4 a_5)/3 + a_5\sigma^2\left(3a_4^2 - b_4^2 - N_c a_4^3 + N_c a_4 b_4^2\right)/6 + b_4\sigma^2\left(-6a_4 b_5 - 2b_4 a_5 - 3\sigma a_4^2 b_5 - \sigma b_5 b_4^2 + 2\sigma a_4 a_5 b_4\right)/6}{\cos(\omega\Delta t)}$$

where $\sigma = c\Delta t/\Delta x$ is the Courant–Friedrichs–Lewy (CFL) number. On checking, the following problems were found with this work:

1. There are no details for the derivation. Therefore, it is difficult to check the correctness of the formula.
2. When σ approaches 0, the formula does not regress to that of the first-order explicit Euler scheme in Eq. (4).
3. When $\omega\Delta t = \pi/2$, the denominator $\cos(\omega\Delta t)$ is 0, and there is a singularity. Therefore, the GRP formula needs further investigation for higher-order Runge–Kutta schemes.

Thus, we employ the idea of [5] and derive the GRP results for high-order Runge–Kutta schemes in Section 3.1.

2.2 ADR method

Despite its applicability to linear schemes, the spectral analysis method by Tam and Webb [1] is unsuitable for nonlinear schemes. Thus, Pirozzoli et al. [2] proposed a quasi-linear spectral analysis method for nonlinear schemes or ADR. The process is as follows [2].

For Eq. (1), suppose the initial distribution is $u(x, 0) = \widehat{u}_0 e^{ikx}$ and consider a semi-discretized approximation of Eq. (1) on grids $\{x_j = j\Delta x\}$ with the spacing Δx as

$$\frac{dv_j}{dt} + c\delta v_j = 0, v_j(0) = \widehat{u}_0 e^{ij\hat{\kappa}}, \tag{6}$$

where $v_j(t) \approx u(x_j, t)$ and δv_j is for a specific numerical scheme, e.g., the linear difference scheme:

$$\delta v_j = \frac{1}{\Delta x} \sum_{l=-N}^{M} a_l u_{j+l},$$

as before. From [2], Eq. (6) has the following exact solution: $v_j(t) = \widehat{v}(t)e^{ij\hat{\kappa}} = \widehat{u}_0 e^{-i(ct/\Delta x)\kappa'} e^{ij\hat{\kappa}}$. Furthermore, Pirozzoli [2] proposed ADR to derive κ':

$$\kappa'\left(\hat{\kappa}_n\right) = \frac{i\Delta x}{c\tau} \ln\left(\frac{\widehat{v}\left(\hat{\kappa}_n, \tau\right)}{\widehat{v}_0\left(\hat{\kappa}_n\right)}\right). \tag{7}$$

In this equation, $\widehat{v}_0\left(\hat{\kappa}_n\right)$ is the Fourier coefficient corresponding to the initial mode and $\widehat{v}\left(\hat{\kappa}_n, \tau\right)$ is the DFT of $v_j(\tau)$ at time τ where $\hat{\kappa}_n = k_n \Delta x$. The operation of DFT is

$$\widehat{v}\left(\hat{\kappa}_n, \tau\right) = \frac{1}{N_x} \sum_{j=0}^{N_x-1} v_j(\tau) e^{-ij\hat{\kappa}_n}, \tag{8}$$

where N_x is the number of grid number.

As indicated in the introduction, ADR depends on the choice of time step and number, and inappropriate choices can lead to temporal errors or unreasonable jump points in the spectral distributions [3]. Mao et al. [3] expanded the solution $v_j(\tau)$ of Eq. (6) with a Taylor series:

$$v_j(\tau) = v_j(0) + \tau \left[-\frac{c}{\Delta x} \sum_{l=-N}^{M} b_{j+l} v_{j+l}(0)\right] + o\left(\tau^2\right).$$

Substituting the above formula into Eq. (8) and the subsequent result into Eq. (7), Mao et al. [3] proposed ADR without time discretization, known as ADR-NT, to derive $\kappa'\left(\hat{\kappa}_n\right)$:

$$\kappa'\left(\hat{\kappa}_n\right) = \frac{1}{i}\left(\sum_{j=0}^{N_x-1}\left(\sum_{l=-N}^{M} b_{j+l} v_{j+l}(0)\right) e^{-ij\hat{\kappa}_n}\right) / \left(N_x \widehat{v}_0\right), \tag{9}$$

where b_{j+l} are the coefficients of the nonlinear scheme.

In order to compare performances by ADR and ADR-NT, the spectral property of WENO5-JS is obtained by the two methods respectively. According to Pirozzoli's advice [2], we set $N_x = 422$ and $\tau = 10^{-8}$ for ADR and the results are shown in Fig. 1. The figure tells that the results of the two methods agree well with each other, which is consistent with that by Mao [2]. Compared with ADR, ADR-NT has reduced the computation cost and the difficulties in deriving the numerical spectrum of schemes. For convenience, ADR-NT is used in this paper.

Fig. 1 $\text{Re}(\kappa')$ of WENO5-JS by ADR and ADR-NT respectively, where $N_x = 422$, $\tau = 10^{-8}$ and RK_4 is used for ADR
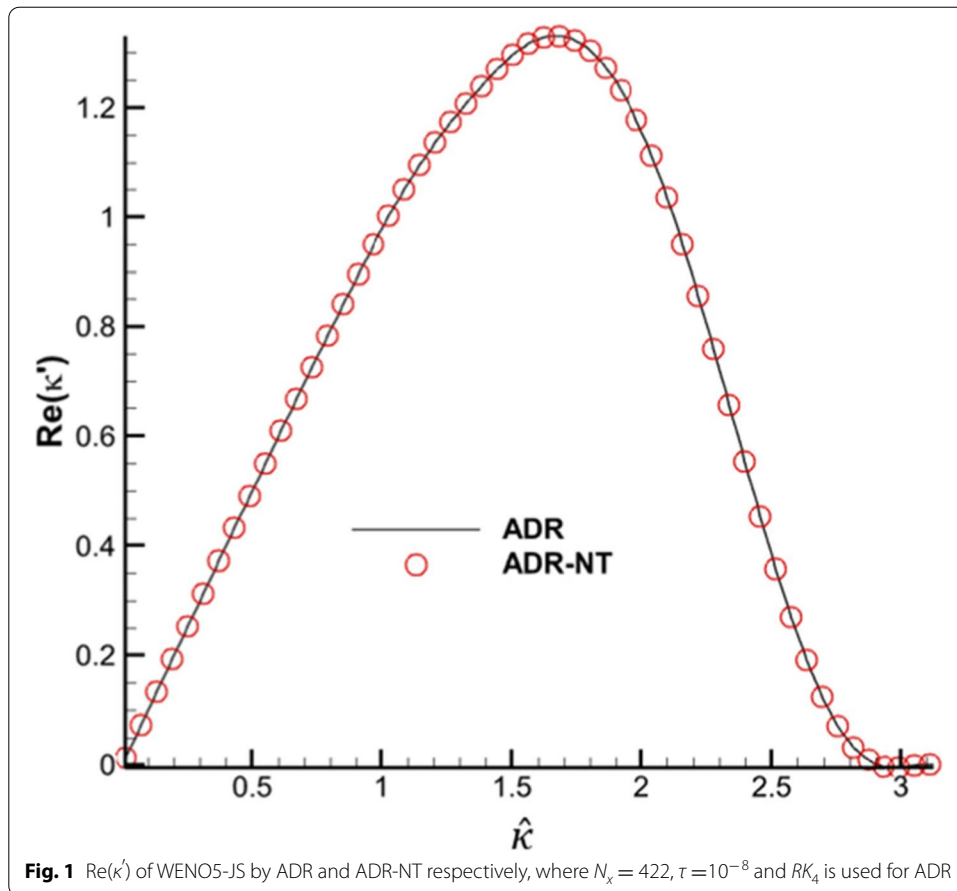
3 QL-GRP for nonlinear schemes

De and Eswaran [5] first analyzed and derived the numerical group velocity for linear schemes. However, their method can be used only for linear schemes and not for nonlinear ones. Considering the development of ADR [2] from DRP [1], which extends the analysis from linear to nonlinear, we introduce the influence of the nonlinearity in GRP [5] by using ADR to account for the spectral property of the nonlinear scheme. Next, employing a similar procedure as in GRP, the so-called QL-GRP is derived for nonlinear schemes. Prior to a further discussion on QL-GRP, we first derive the GRP formula for high-order Runge–Kutta schemes.

3.1 GRP formula for high-order Runge–Kutta schemes

Taking the third-order Runge–Kutta scheme as an example, we derive the GRP formula based on the method of [5]. For convenience, the nth-order Runge–Kutta scheme is referred to as RK_n.

RK_3 here takes the form [7]:

$$\begin{cases} u^{(1)} = u^n + \Delta t \cdot f(u^n), \\ u^{(2)} = \frac{3}{4}u^n + \frac{1}{4}u^{(1)} + \frac{1}{4}\Delta t \cdot f\left(u^{(1)}\right), \\ u^{n+1} = \frac{1}{3}u^n + \frac{2}{3}u^{(2)} + \frac{2}{3}\Delta t \cdot f\left(u^{(2)}\right), \end{cases} \tag{10}$$

where $f(u^n)$, $f(u^{(1)})$, and $f(u^{(2)})$ are the derivatives on the sub-time steps. From Eq. (10), u^{n+1} can be reformulated as:

$$u^{n+1} = u^n + \Delta t \left(\frac{1}{6} f\left(u^{(n)} \right) + \frac{1}{6} f\left(u^{(1)} \right) + \frac{2}{3} f\left(u^{(2)} \right) \right).$$

Let $K_1 = f(u^{(n)})$, $K_2 = f(u^{(1)})$, and $K_3 = f(u^{(2)})$. Then, Eq. (2) can be rewritten as:

$$\widehat{u}e^{i[kx-\omega(t+\Delta t)]} - \widehat{u}e^{i(kx-\omega t)} \approx \Delta t \cdot \left(\frac{1}{6}K_1 + \frac{1}{6}K_2 + \frac{2}{3}K_3 \right). \tag{11}$$

It is known that K_1 in Eq. (10) corresponds to the derivative of u^n or $K_1 = f(t^n, u^n)$; similarly $K_2 = f(t^n + \Delta t, u^{(1)}) = f(t^n + \Delta t, u^n + \Delta t K_1)$ and $K_3 = f\left(t^n + \frac{1}{2}\Delta t, u^n + \frac{1}{2}\Delta t \cdot \frac{1}{2}(K_1 + K_2) \right)$. Using κ', then K_i in Eq. (11) can be written as [5, 8]:

$$\begin{cases} K_1 = (-c) \cdot \frac{i\kappa'}{\Delta x} \widehat{u}e^{i(kx-\omega t)}, \\ K_2 = \left[(-c) \cdot \frac{i\kappa'}{\Delta x} + \Delta t \cdot (-c^2)\left(\frac{\kappa'}{\Delta x} \right)^2 \right] \widehat{u}e^{i(kx-\omega t)}, \\ K_3 = \left[(-c) \cdot \frac{i\kappa'}{\Delta x} + \frac{\Delta t}{4} \cdot (-c^2)\left(\frac{\kappa'}{\Delta x} \right)^2 + \frac{\Delta t}{4}\left((-c^2)\left(\frac{\kappa'}{\Delta x} \right)^2 + \Delta t \cdot ic^3 \left(\frac{\kappa'}{\Delta x} \right)^3 \right) \right] \widehat{u}e^{i(kx-\omega t)}. \end{cases} \tag{12}$$

Substituting Eq. (12) into Eq. (11):

$$e^{-i\omega\Delta t} - 1 \approx -i\sigma \cdot \kappa' - \frac{1}{2}(\sigma \cdot \kappa')^2 + \frac{1}{6}i(\sigma \cdot \kappa')^3.$$

Applying $d(.)/dk$ to the above equation and taking the real part as in [5], the group velocity for RK_3 is

$$\left(V_{g,num} \right)_{RK_3} = c \cdot \mathrm{Re}\left(\left(1 - i\sigma \cdot \kappa' - \frac{1}{2}(\sigma \cdot \kappa')^2 \right) e^{i\omega\Delta t} \cdot \frac{d\kappa'}{d\hat{\kappa}} \right). \tag{13}$$

For a linear scheme, κ' is found from Eq. (5) [5]. Similarly, when an RK_4 scheme is used for time discretization, the GRP formula can be derived as:
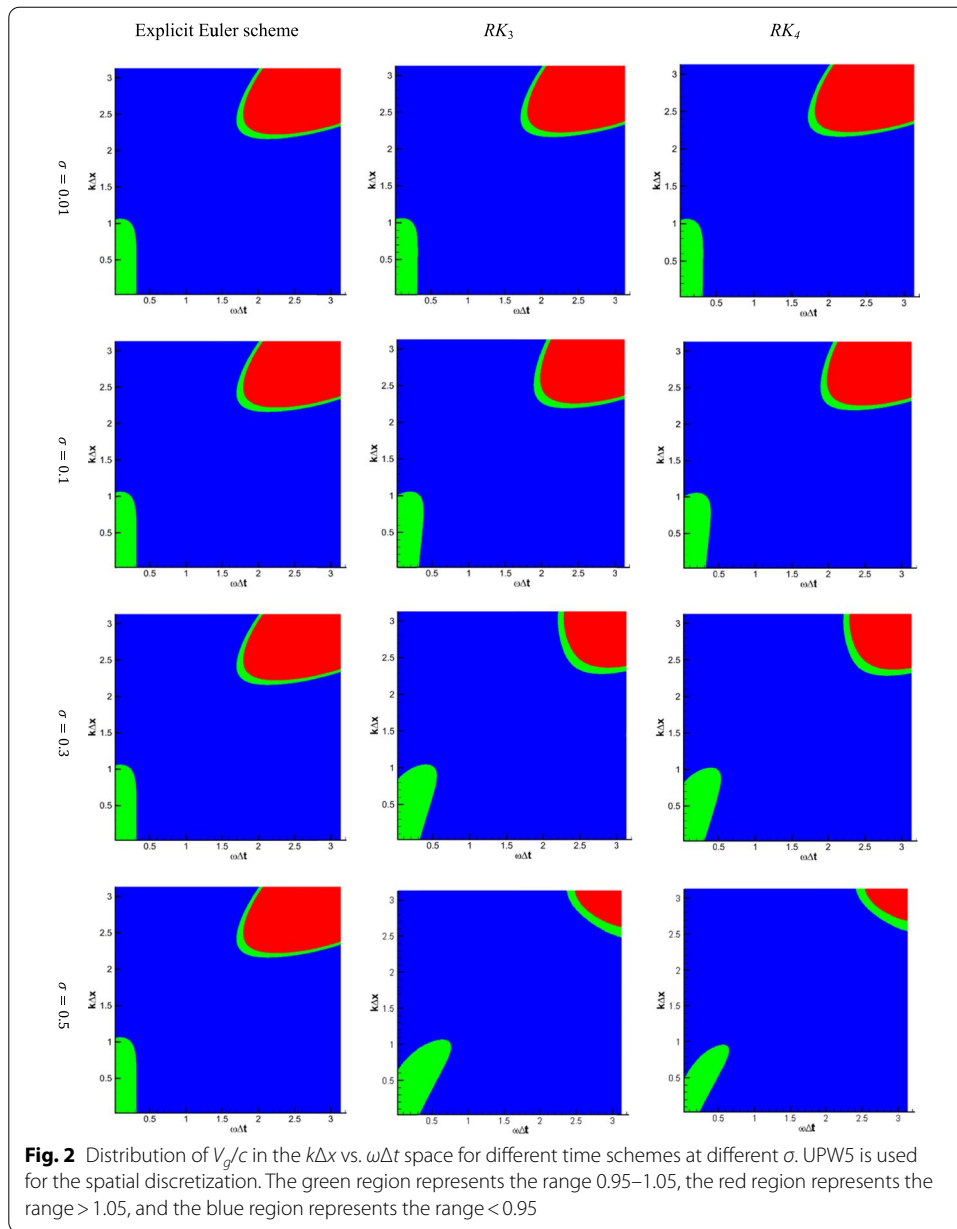
$$\left(V_{g,num} \right)_{RK_4} = c \cdot \mathrm{Re}\left(\left(1 - i\sigma \cdot \kappa' - \frac{1}{2}(\sigma \cdot \kappa')^2 + \frac{1}{6}i(\sigma \cdot \kappa')^3 \right) e^{i\omega\Delta t} \cdot \frac{d\kappa'}{d\hat{\kappa}} \right). \tag{14}$$

From Eqs. (13) and (14), it can be seen that the numerical group velocity for a high-order Runge–Kutta scheme depends on σ, unlike the first-order explicit Euler scheme in Eq. (4). For illustration, the group velocity of a linear fifth-order scheme, UPW5, namely:

$$(du/dx)_j \approx \frac{1}{\Delta x}\left(-\frac{1}{30}u_{i-3} + \frac{1}{4}u_{i-2} - u_{i-1} + \frac{1}{3}u_i + \frac{1}{2}u_{i+1} - \frac{1}{20}u_{i+2} \right),$$

was investigated for different CFL numbers. The velocity distributions are shown in Fig. 2 for $\sigma = 0.01$, 0.1, 0.3 and 0.5, respectively. The effect of σ is apparent through the variation of the GVP region, for which $V_{g,num}/c \in [0.95, 1.05]$, as mentioned before.

As indicated by De and Eswaran [5], the group velocity distribution near the origin is of special concern. Because the region where V_g/c lies in (0.95,1.05) is of

Fig. 2 Distribution of V_g/c in the $k\Delta x$ vs. $\omega\Delta t$ space for different time schemes at different σ. UPW5 is used for the spatial discretization. The green region represents the range 0.95–1.05, the red region represents the range > 1.05, and the blue region represents the range < 0.95

the major point, they [4, 5] divided the domain into three regions with the value ranges as < 0.95, 0.95 ~ 1.05, and > 1.05 to highlight the GVP region of schemes. In terms of the similar consideration, the same choice is used in this paper. Figure 2 shows that when the CFL number is small, the distributions of the first-order explicit Euler scheme, RK_3, and RK_4 are almost the same. With an increase of the CFL number, differences appear among the different time schemes. As shown in Fig. 2, when $\sigma = 0.1$, for the green area near the origin, $RK_4 \approx RK_3 >$ the explicit Euler scheme, which indicates that higher-order time schemes enhance the GVP. This outcome confirms the potential advantages of higher-order time schemes for

unsteady problems. With the further increase of σ, GVP regions of RK_3 and RK_4 change apparently due to the inclusion of σ in Eqs. (13) and (14), which is qualitatively consistent with that in [5].

In summary, in this section the group velocities of RK_3 and RK_4 were found by applying the same procedure used for the explicit Euler scheme in [5]. The following remarks are given: (1) When the CFL number approaches 0, the group velocity distributions of higher-order Runge–Kutta schemes gradually degenerate into that of the first-order explicit Euler scheme. Further, the results from GRP for different time schemes become the same under this condition. (2) No singularity arises in Eqs. (13) and (14), which indicates their rationality.

3.2 QL-GRP

As mentioned in the introduction, QL-GRP is proposed to evaluate the characteristics of the group velocity in a quasi-linear manner. The main difference between QL-GRP and GRP is that the modified wave number in the former considers the nonlinearity of schemes. Therefore, the formulas for QL-GRP are the same as those for GRP, such as Eqs. (13) or (14), except that different evaluations of κ' are implemented.

The concrete implementations are summarized as follows:

1. Solve for the modified wave number $\kappa'(\hat{\kappa})$ of nonlinear spatial schemes.

Based on ADR, the dispersion and dissipation relations of the nonlinear scheme, $\kappa'(\hat{\kappa})$, are solved with Eq. (9).

2. Solve for $d\kappa'/d\hat{\kappa}$.

When the spatial scheme is linear, $\kappa'(\hat{\kappa})$ can be obtained as $\kappa'(\hat{\kappa}) = -i \sum\limits_{j=-N}^{M} a_j e^{ij\hat{\kappa}}$. Because the coefficient a_j is constant, $d\kappa'/d\hat{\kappa}$ can be derived analytically. However, when the spatial scheme is nonlinear, the coefficient b_{j+l} in Eq. (9) correlates with the initial variable distribution nonlinearly and $d\kappa'/d\hat{\kappa}$ is hard to resolve analytically. To overcome this difficulty, we use the difference method to evaluate it numerically. Taking the second-order central difference as an example, $d\kappa'/d\hat{\kappa}$ can be evaluated as:

$$\left(\frac{d\kappa'}{d\hat{\kappa}}\right)_j \approx \frac{1}{60\Delta\hat{\kappa}}\left(-\kappa'_{j-3} + 9\kappa'_{j-2} - 45\kappa'_{j-1} + 45\kappa'_{j+1} - 9\kappa'_{j+2} + \kappa'_{j+3}\right), \qquad (15)$$

where j is the index of the reduced wave number and

$$\hat{\kappa}_j = k_j\Delta x = \frac{2\pi}{\lambda_j} \times \frac{L}{j} = \frac{2\pi j}{N_x},$$

for $j = 0, ..., N_x/2$.

3. Substitute $d\kappa'/d\hat{\kappa}$ into the QL-GRP formulas, such as Eqs. (13) or (14), to obtain $V_{g,num}$.

When solving for $\kappa'(\hat{\kappa})$ for nonlinear schemes with ADR, Δt in the time integration must be small enough [2], which means the corresponding reduced frequency $\omega\Delta t$ should also be small. Correspondingly, QL-GRP can describe the GVP of nonlinear schemes effectively only for a small reduced frequency. When $\omega\Delta t$ is large, ADR does not accurately predict the spectral property, and therefore, QL-GRP cannot accurately describe GVP either. However, QL-GRP can give some insights into the group velocity of a nonlinear scheme. Hence, QL-GRP can provide a useful reference for the overall characteristics of the group velocity for a nonlinear scheme.
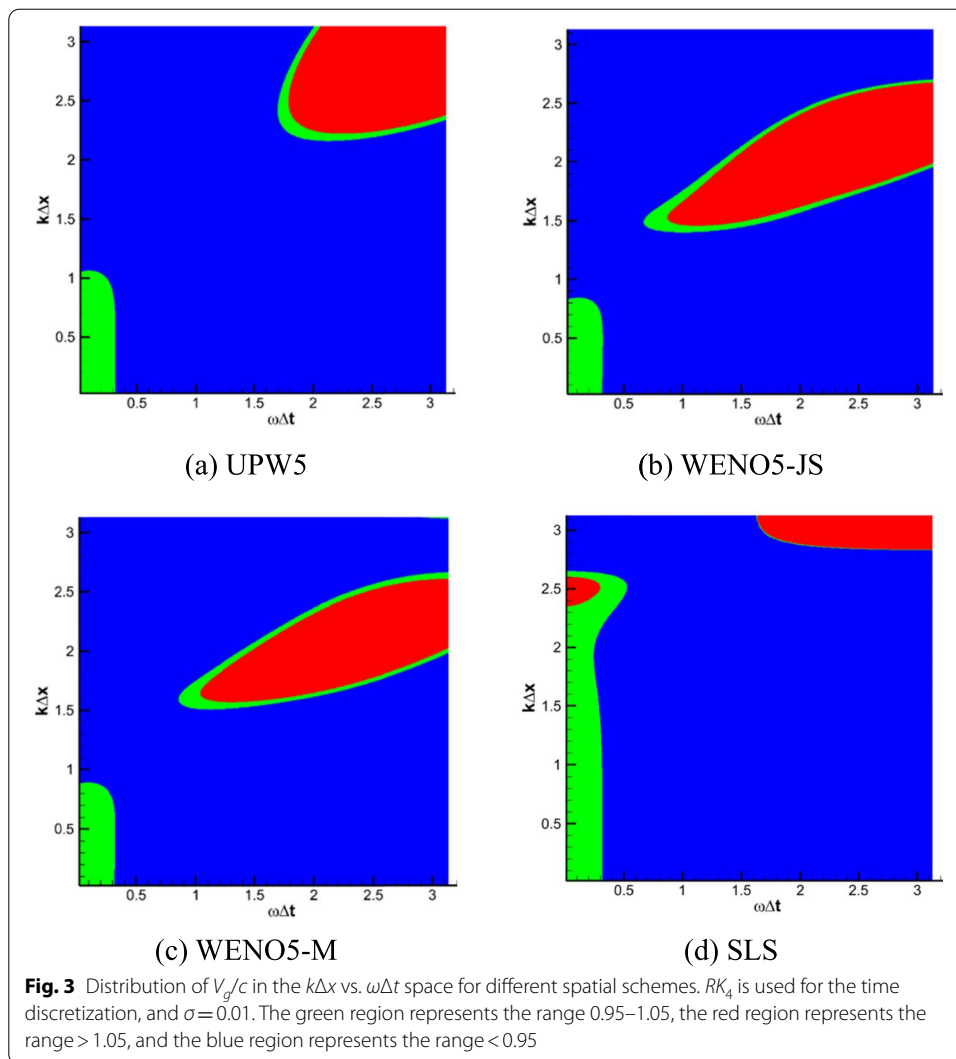
For demonstration, we used QL-GRP to find the group velocity for three typical spatial schemes: UPW5, WENO5-JS [7], and WENO5-M [9]. Besides, in order to show the difference of GVP regions more obviously, the optimized SLS scheme [8], $0.0895(u'_{i-2} + u'_{i+2}) + 0.57967(u'_{i-1} + u'_{i+1}) + u'_i \approx \frac{1}{\Delta x}\left[0.00559(u_{i+3} - u_{i-3}) + 0.25154(u_{i+2} - u_{i-2}) + 0.6494(u_{i+1} - u_{i-1}) \right]$, which has smaller dispersion error and optimized spectral property is investigated. Adopting the aforementioned procedure, the corresponding distributions of V_g/c with the RK_4 scheme are shown in Fig. 3.

The figure shows that:

1. Comparing Fig. 3a with Fig. 2, one can see that the group velocity distributions for QL-GRP with the UPW5 scheme are the same as those for GRP. This is because, for linear schemes, $\kappa'(\hat{\kappa})$ in ADR is the same as that in DRP [1]. In other words, QL-GRP degenerates into GRP for a linear spatial scheme.
2. The distributions of the group velocity are obviously different for the four schemes, which indicates that QL-GRP can be used to distinguish between the GVP of different spatial schemes under the same time scheme. Specifically, the area of the GVP region (green) for the WENO5-JS scheme is smaller than that for the UPW5 scheme, which indicates that the group velocities of the nonlinear scheme differ from that of the linear scheme. Moreover, the GVP area of the WENO5-M scheme is larger than that of WENO5-JS, which shows that the nonlinear optimization of the former enhances the GVP. Among the schemes in Fig. 3, SLS obviously yields the largest GVP region, which is consistent with its excellent spectral property than other three schemes.
3. The GVP area near the origin, especially along the vertical axis, is the largest for SLS, followed by UPW5, then WENO5-M and finally WENO5-JS.

In short, QL-GRP can be applied not only to analyze the group velocity of a linear scheme but also of a nonlinear scheme. Moreover, the method can clearly differentiate spatial schemes by considering the size of the GVP region.

Despite the presentation of QL-GRP and its capability to tell the differences of nonlinear schemes on GRP, how to use it to optimize difference schemes is not indicated at present. One may observe that DRP can be well used in scheme optimizations as shown in [10, 11]. In this regard, an analogous occurrence can be noticed that ADR [2, 3],

Fig. 3 Distribution of V_g/c in the $k\Delta x$ vs. $\omega\Delta t$ space for different spatial schemes. RK_4 is used for the time discretization, and $\sigma = 0.01$. The green region represents the range 0.95–1.05, the red region represents the range > 1.05, and the blue region represents the range < 0.95

although its less use in scheme optimization, is widely accepted and applied to evaluate the spectral properties of nonlinear schemes, and hopefully QL-GRP would play a similar role. Besides, as indicated in above, different nonlinear schemes yield different GVP regions, which might be used in scheme optimization and would be discussed in other investigations.

4 Numerical analysis and validation of QL-GRP

The previous section introduced the derivation and implementation of QL-GRP. In this section, the numerical group velocity is obtained numerically and the results are compared with those from QL-GRP. Thus, the rationality of the method will be analyzed and verified. Moreover, we devise hyperbolic equations and a corresponding example to determine the numerical group velocity of the scheme directly, which further verifies the approach.

4.1 Numerical analysis and validation

In this section, the group velocity of different schemes is numerically obtained by solving the one-dimensional wave propagation equation and by using DFT. By comparing with the analytic results from QL-GRP, the numerical error is acquired and the rationality of QL-GRP is evaluated.

First, we select several points P_i in the $k\Delta x$ vs. $\omega\Delta t$ plane, then numerically compute the group velocity using DFT. The coordinates of P_i are the reduced frequency and wave number. Without loss of generality, we set $k\Delta x$ as 1. Because $\omega = kc$, then

$$\omega\Delta t = c\frac{\Delta t}{\Delta x}\hat{\kappa}.$$

Hence, once Δt and Δx are determined, the coordinates of P_i are defined.

Next, the derivation of numerical group velocity will be discussed. The solution of the semi-discrete Eq. (6) is

$$v_j(t) = \widehat{u}_0 e^{-i(ct/\Delta x)\kappa'} e^{ij\hat{\kappa}} = \widehat{u}_0 \exp\left[i\left(kx - \frac{c\kappa'}{\Delta x}t\right)\right]$$

where $\kappa' = \kappa'(\hat{\kappa})$ [12]. Compared with the exact solution $u_j(t) = \widehat{u}_0 e^{i(kx-\omega t)}$, the numerical frequency can be expressed as $\omega' = c\kappa'/\Delta x$, which depends on κ'. Hence, the reduced frequency at P_i can be expressed with the modified wave number as:

$$\omega'\Delta t = c\frac{\kappa'\Delta t}{\Delta x} = c\kappa'\frac{N\Delta t}{L}, \tag{16}$$

where L is the length of the computational domain. We consider Eq. (1) with $c=1$ and the initial distribution $u_0 = \cos(x)$ at $x \in [0, L]$ with $L = 2\pi$. From [2], κ' can be numerically found with ADR [2] for a spatial scheme and time scheme using DFT. Here, we use WENO5-JS and RK_4 for the spatial and time discretization. The number of grid cells and time step are given in Table 1. As shown in the table, four cases with respective $(N_x, \Delta t)$ are chosen, and these correspond to P_i. Then, κ' can be acquired with respect to $\hat{\kappa}$, as illustrated in Fig. 4.
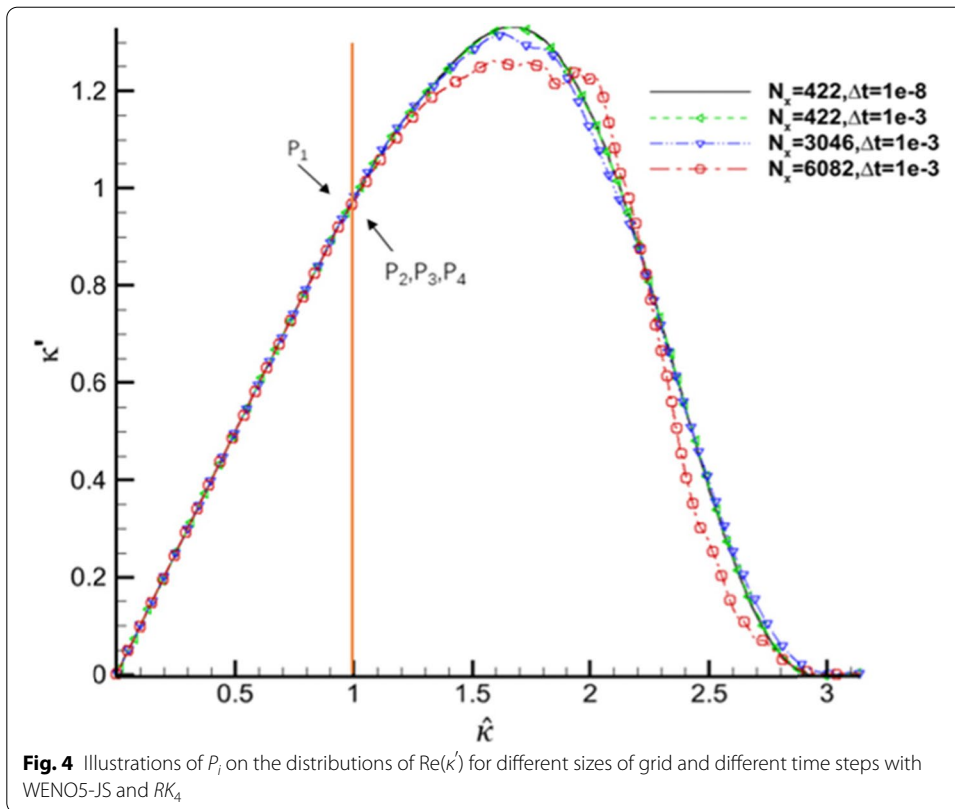
Besides P_1 to P_4, we also investigated the case when the reduced frequency was larger. There were oscillations in the results. Hence, the frequency region for investigation was limited to $\omega\Delta t < 1$. For illustration, the positions of P_i ($i = 1, 2, 3, 4$) are shown in the $k\Delta x$ vs. $\omega\Delta t$ plane in Fig. 5. The colors indicate the group velocity calculated by QL-GRP with WENO5-JS and RK_4.

Thus far, the numerical solution of the group velocity can be found from:

$$V_{g,num} = \text{Re}\left(\Delta\omega'\right)/\Delta k = \text{Re}\left(\omega_2' - \omega_1'\right)/(k_2 - k_1), \tag{17}$$

Table 1 Size of computational grid, time step, and coordinates of P_i

Point	Grid number N_x	Time step, Δt	$(k\Delta x, \omega\Delta t)$
P_1	422	10^{-8}	$(1, 6.72 \times 10^{-7})$
P_2	422	10^{-3}	$(1, 0.0672)$
P_3	3046	10^{-3}	$(1, 0.04848)$
P_4	6082	10^{-3}	$(1, 0.968)$

Fig. 4 Illustrations of P_i on the distributions of Re(κ') for different sizes of grid and different time steps with WENO5-JS and RK_4

where k_1 and k_2 represent two wave numbers with a small difference, ω'_1 and ω'_2 are the corresponding numerical frequencies, and Re denotes taking the real part. Substituting Eq. (16) into Eq. (17):

$$V_{g,num} = \frac{\text{Re}\left(\kappa'_2\left(\hat{\kappa}_2\right) - \kappa'_1\left(\hat{\kappa}_1\right)\right)}{\hat{\kappa}_2 - \hat{\kappa}_1}. \tag{18}$$

Under the assumption that $\hat{\kappa} = 1$ as above, we set $\hat{\kappa}_1$ and $\hat{\kappa}_2$ as $\hat{\kappa}_1 = 1 - \Delta\hat{\kappa}$ and $\hat{\kappa}_2 = 1 + \Delta\hat{\kappa}$. The corresponding modified wave numbers Re($\kappa'_1\left(\hat{\kappa}_1\right)$) and Re($\kappa'_2\left(\hat{\kappa}_2\right)$) can be obtained from the distributions of Re(κ') in Fig. 4. Moreover, $V_{g,\ num}$ is the slope of Re(κ') at the point $\left(1, \kappa'_i(1)\right)$.

Next, we compare the group velocities at P_i obtained by QL-GRP and the numerical analysis. For QL-GRP, the analytic group velocity $V_{g,\ anal}$ at P_i can be obtained from Eqs. (9) and (14), whereas the numerical group velocity $V_{g,\ num}$ at P_i can be obtained from Eq. (18). These are compared in Table 2.

Table 2 shows that when $\omega\Delta t$ is small, as for P_1, P_2, and P_3, then the group velocity given by QL-GRP is quite close to the numerical value. This indicates that QL-GRP can reasonably predict the group velocity at low reduced frequency. With an increase of $\omega\Delta t$, the error between $V_{g,\ anal}$ and $V_{g,\ num}$ becomes large but is still within 21% when $\omega\Delta t < 1$. Therefore, QL-GRP can provide important insights for the group velocity at medium reduced frequency.
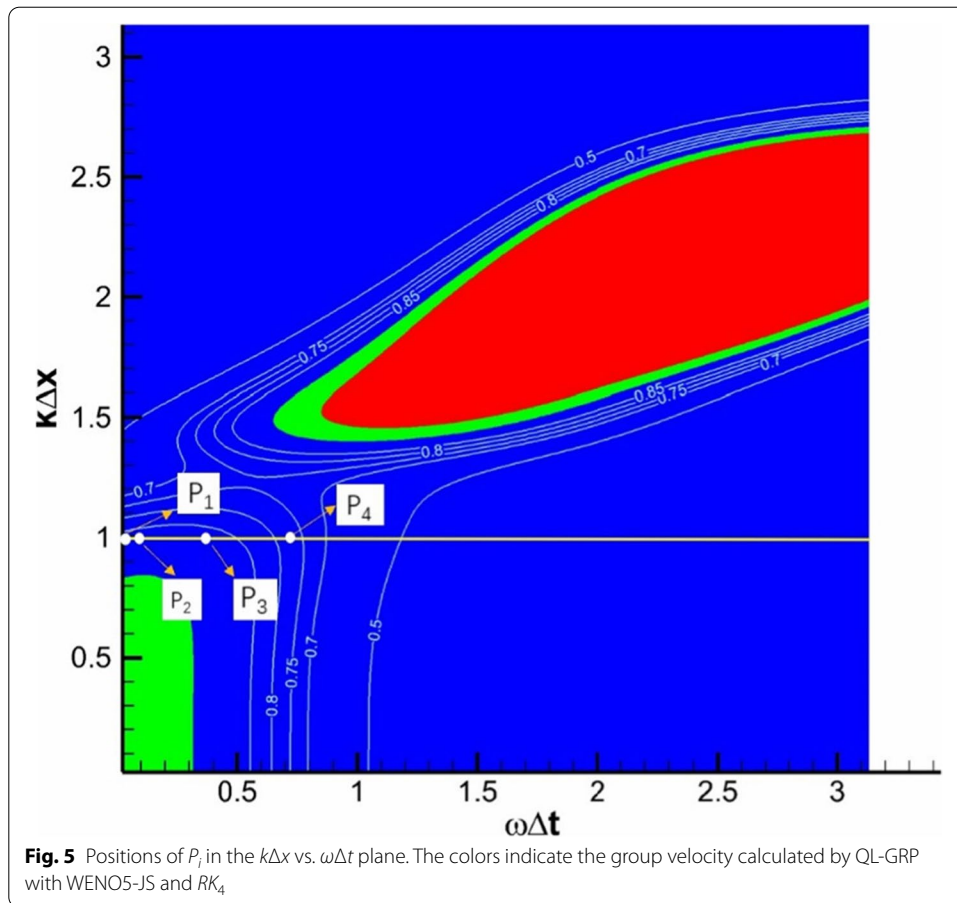
Fig. 5 Positions of P_i in the $k\Delta x$ vs. $\omega\Delta t$ plane. The colors indicate the group velocity calculated by QL-GRP with WENO5-JS and RK_4

Table 2 Both group velocities and errors of P_i for WENO5-JS and RK_4

Point	$V_{g, num}$	$V_{g, anal}$	$|V_{g, anal} - V_{g, num}|/V_{g, num}$
P_1	0.8647	0.8627	0.23%
P_2	0.8638	0.8698	0.69%
P_3	0.8732	0.8524	2.38%
P_4	0.8203	0.6505	20.70%

Note that QL-GRP can provide an overview of the group velocity in the $k\Delta x$ vs. $\omega\Delta t$ space, which is difficult for the numerical approach just mentioned. In addition, QL-GRP avoids the tedious process of finding a numerical solution and is more convenient for practical analyses.

4.2 Constructing hyperbolic equations for a combination wave with different phase and group velocities

The distribution $u = \cos(kx - \omega t)$ satisfies Eq. (1) when $\omega/k = c$, where the group and phase velocities are $V_{g, exact} = d\omega/dk = c$ and $V_{p, exact} = \omega/k = c$, respectively. One can

see that in such situations, the group velocity and phase velocity are indistinguisha-ble, which is unfavorable for investigating the GVP property of the numerical scheme.

In textbooks, the combination wave $u = \cos(k_1 x - \omega_1 t) + \cos(k_2 x - \omega_2 t)$ is usually used to explain the concept of group velocity, which can also be written as:

$$u = 2 \cos\left(\frac{k_1 + k_2}{2} x - \frac{\omega_1 + \omega_2}{2} t\right) \cos\left(\frac{k_2 - k_1}{2} x - \frac{\omega_2 - \omega_1}{2} t\right). \tag{19}$$

The envelope of Eq. (19) is

$$2 \cos\left(\frac{k_2 - k_1}{2} x - \frac{\omega_2 - \omega_1}{2} t\right),$$

and the corresponding group velocity and phase velocity are

$$V_{g,exact} = \frac{\omega_2 - \omega_1}{k_2 - k_1} \quad \text{and} \quad V_{p,exact} = \frac{\omega_2 + \omega_1}{k_2 + k_1}.$$

Without loss of generality, it is usually assumed that $k_1 = \omega_1$. When $k_2 \neq \omega_2$, then $V_g \neq V_p$.

Although the combination wave is used to explain the group velocity and phase veloc-ity, the distribution does not satisfy Eq. (1). Therefore, this equation cannot be used to simulate the wave. We devised the following hyperbolic equations so that we could numerically study the GVP of different schemes:

$$\begin{cases} \frac{\partial u}{\partial t} + \frac{\partial u}{\partial x} = p, \\ \frac{\partial p}{\partial t} + a \frac{\partial p}{\partial x} = 0. \end{cases} \tag{20}$$

It can be shown that Eq. (19) satisfies Eq. (20) and $a = \omega_2/k_2$ when $k_1 = \omega_1$. If $a \neq 1$, the group velocity is different from the phase velocity. Hence, a measure is provided to study the combination wave with the co-occurrence of different group and phase velocities, which also provides a powerful way to verify the outcome of QL-GRP.

5 Numerical examples

In the following, to compute the group velocity, the envelope of the wave is derived by a Hilbert transform.

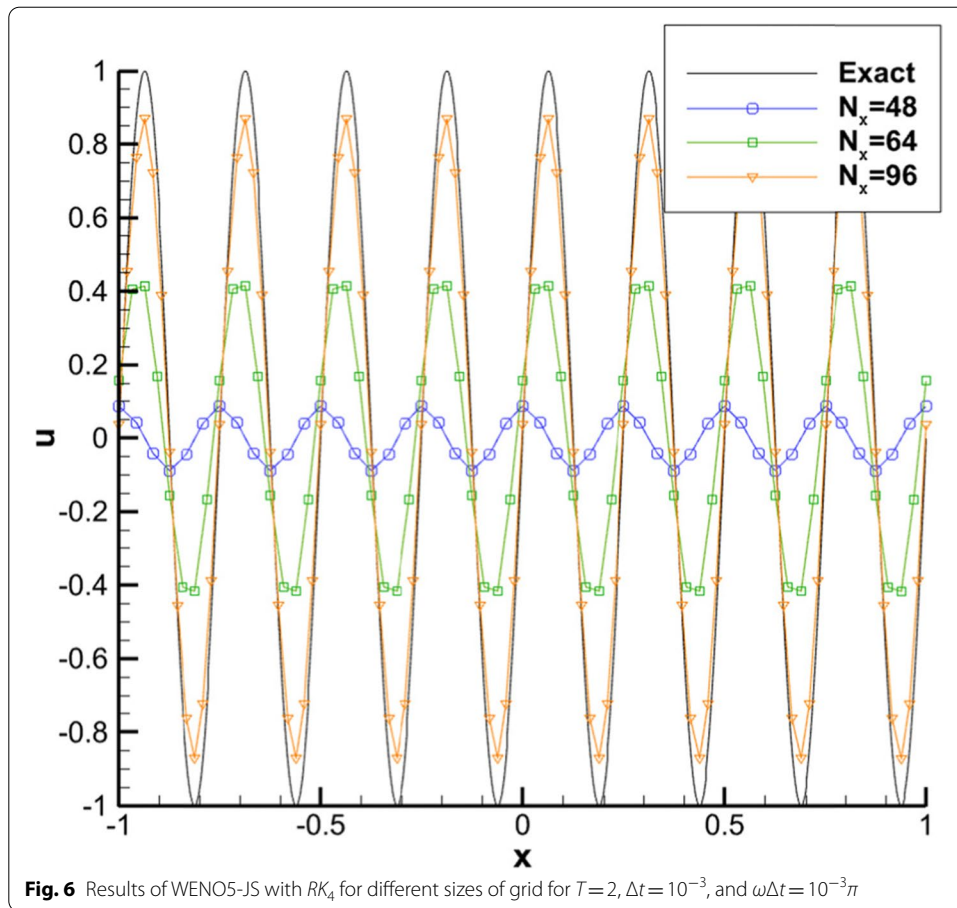### 5.1 One-dimensional wave propagation

(1) Initial condition using sinuous distribution

Consider Eq. (1) with $c = 1/8$. The following initial distribution is chosen:

$$u_0 = \sin(8\pi x). \tag{21}$$

The exact solution is $u = \sin(8\pi x - \pi t)$ with $V_{g,\,exact} = V_{p,\,exact} = 1/8$.

Two tests were used to check the GVP: (1) using the same spatial scheme for dif-ferent $\hat{\kappa}$ and (2) using different spatial schemes for the same $\hat{\kappa}$. Considering that

Fig. 6 Results of WENO5-JS with RK_4 for different sizes of grid for $T=2$, $\Delta t=10^{-3}$, and $\omega\Delta t=10^{-3}\pi$
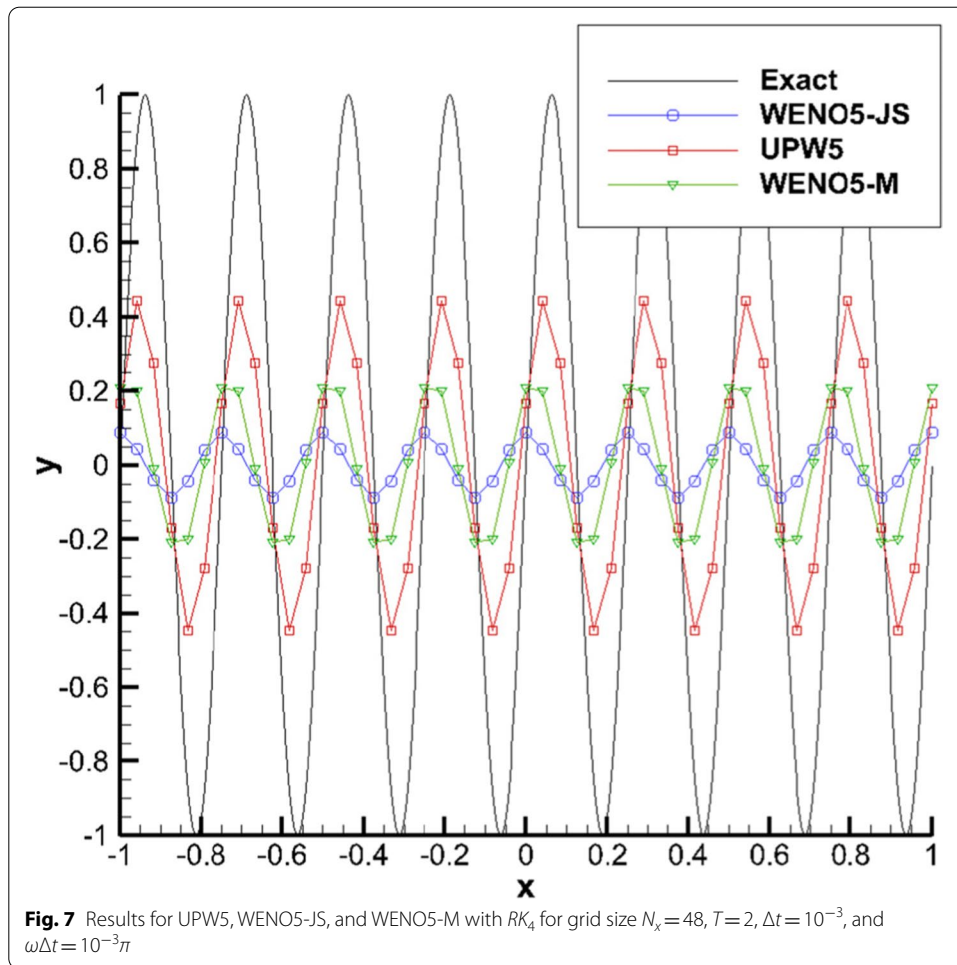
$\hat{\kappa} = k\Delta x = kL/N_x$, $\hat{\kappa}$ can be adjusted by changing the size of N_x. In the computation, $T=2$, $\Delta t=10^{-3}$, and $\omega\Delta t=10^{-3}\pi$, and the computational domain was $[-1, 1]$.

First, the performance of WENO5-JS was tested for different grids, as shown in Fig. 6.

When N_x was 48, 64, or 96, $\hat{\kappa}$ was $\pi/3$, $\pi/4$, or $\pi/6$, respectively. Because the group velocity is equal to the phase velocity in this situation, the phase velocity can be computed by the phase change of the wave peak, and the group velocity can be obtained thereafter. Figure 6 shows that when $\hat{\kappa} = \pi/3$, the numerical group velocity was about 0.1025 and the ratio $V_{g,\,num}/V_{g,\,exact}=0.82$. When $\hat{\kappa} = \pi/4$, $V_{g,\,num}$ was about 0.11875 and $V_{g,\,num}/V_{g,\,exact}=0.95$, which indicated that the group velocity was in the accurate region $[0.95, 1.05]$. With an increase of N_x, $\hat{\kappa}$ decreased and the numerical group velocity gradually approached the theoretical value, i.e., $V_{g,\,num}$ was 0.99 when $\hat{\kappa} = \pi/6$.

Using QL-GRP with the WENO5-JS scheme and the RK_4 scheme, for the same three points $(\pi/3, 10^{-3}\pi)$, $(\pi/4, 10^{-3}\pi)$, and $(\pi/6, 10^{-3}\pi)$ in the $k\Delta x$ vs. $\omega\Delta t$ plane, $V_{g,\,num}/V_{g,\,exact}$ can be derived from Eq. (14) as 0.8259, 0.9592, and 0.9950, respectively. These values are nearly the same as those obtained numerically. Hence, QL-GRP has been verified quantitatively, and its usefulness in analyses of the group velocity has been demonstrated.

Fig. 7 Results for UPW5, WENO5-JS, and WENO5-M with RK_4 for grid size $N_x = 48$, $T = 2$, $\Delta t = 10^{-3}$, and $\omega \Delta t = 10^{-3}\pi$

Next, GVP was compared for UPW5, WENO5-JS, and WENO5-M for $N_x = 48$ and $(\hat{\kappa}, \omega \Delta t) = (\pi/3, 10^{-3}\pi)$. The results are shown in Fig. 7.

Figure 7 shows that the UPW5 scheme yields a relatively accurate group velocity, since $V_{g,\,num}/V_{g,\,exact} = 0.96$, whereas WENO5-M and WENO5-JS have relatively large errors, i.e., $V_{g,\,num}/V_{g,\,exact} = 0.87$ and 0.82, respectively. WENO5-M performed better than WENO5-JS. The rank of performance for the GVP is UPW5 > WENO5-M > WENO5-JS. The results for QL-GRP are consistent with the numerical results, which demonstrates the validity and capability of QL-GRP for nonlinear schemes.

(2) Initial condition using wave packet-like distribution

Consider Eq. (1) with $c = 1$. The following initial distribution is chosen:

$$u_0 = \cos(7x) \times \cos^6(x). \tag{22}$$
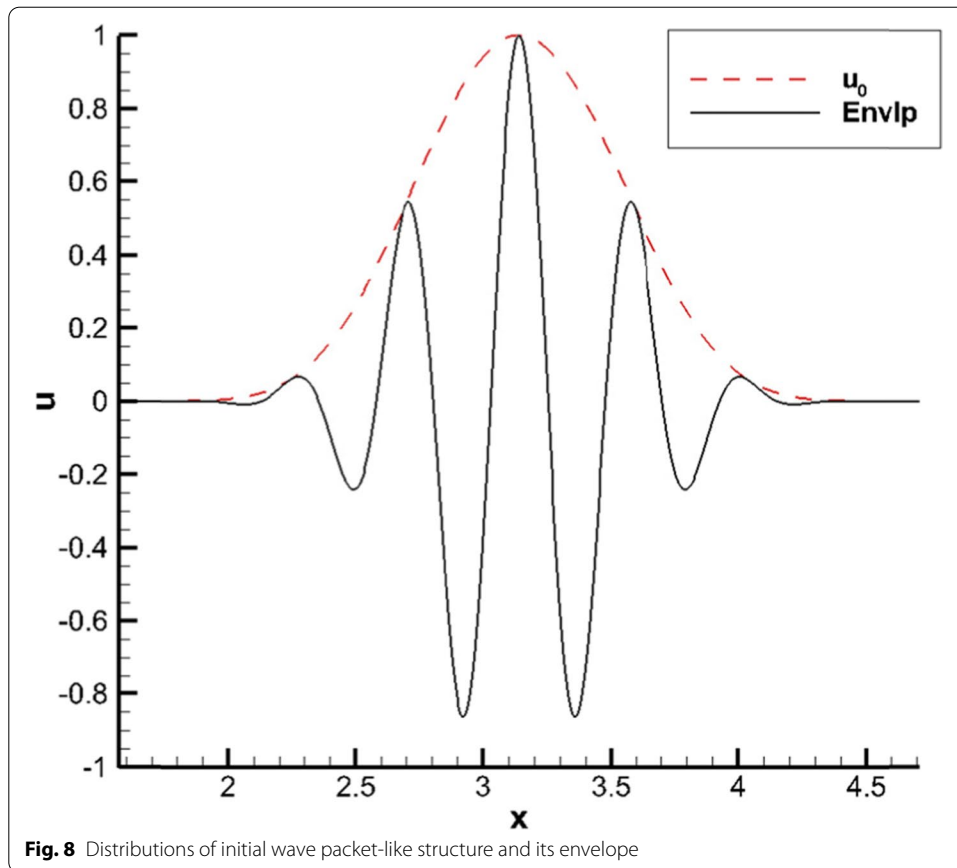
Fig. 8 Distributions of initial wave packet-like structure and its envelope

The period of the distribution can be found as π. For brevity, the "envelope" in the following figures is abbreviated as "envlp". The initial distribution which imitates a wave packet-like structure and its envelope are shown in Fig. 8. Note that due to the employment of Eq. (1) as the governing equation, the group speed here is still the same as the phase velocity.

The same three spatial schemes as above, UPW5, WENO5-M, and WENO5-JS, are tested to further explore their GVP. In the computation, $T = \pi$, $\Delta t = 10^{-3}$, $N_x = 48$, and the computational domain was $[\pi/2, 3\pi/2]$. The results are shown in Fig. 9 with envelopes derived.

From the figure, it can be seen that UPW5 yields the most accurate group velocity in three schemes, which is followed by WENO5-M, whose peak value of envelope has decreased from the exact "1" to "0.4". WENO5-JS has the least performance considering its smallest and deformed envelope. The rank of GVP performance is still: UPW5 > WENO5-M > WENO5-JS, as indicated by previous QL-GRP analysis.

5.2 Wave propagation with different group and phase velocities

In this section, the case described in Section 4.2 with different group and phase velocities is evaluated for the different spatial schemes, namely UPW5, WENO5-M, and WENO5-JS, which further demonstrates the validity of QL-GRP.

Fig. 9 Solution distributions and corresponding envelopes for $T=\pi$ under the initial packet-like wave and the conditions $N_x=48$ and $\Delta t=10^{-3}$ for different spatial schemes and RK_4
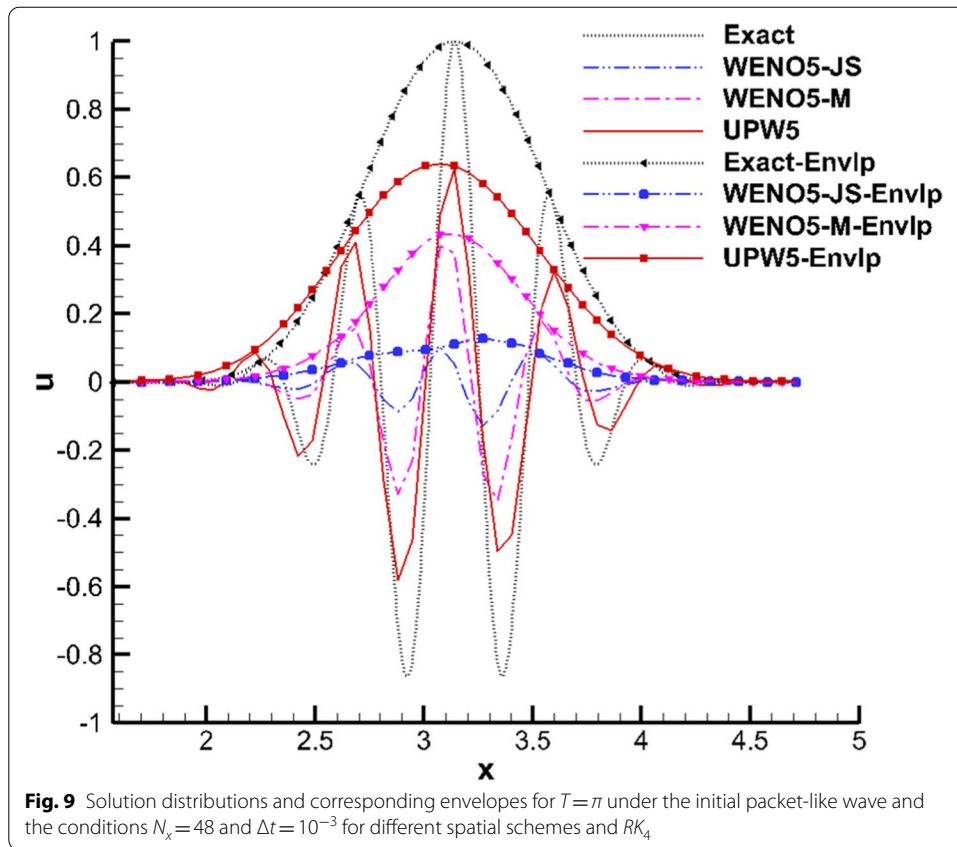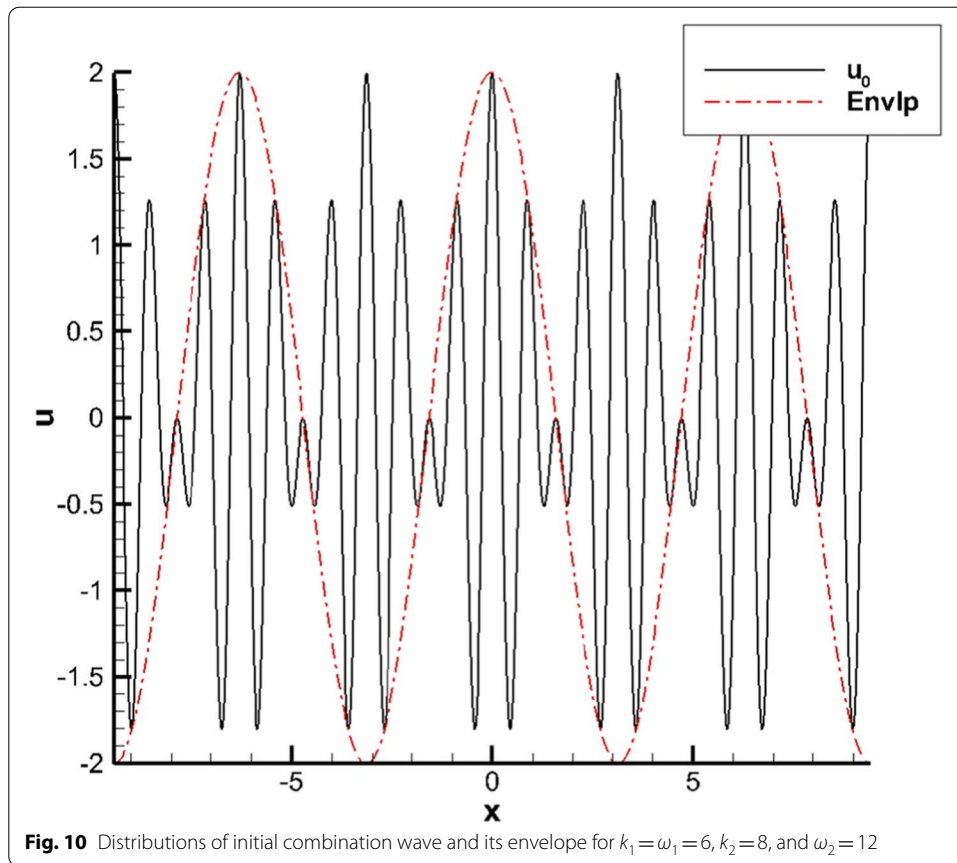
For the distribution in Eq. (19), multiple waves were included in one wave packet for the purpose of better illustration. The initial condition is

$$u_0 = 2\cos\left(\frac{k_1 + k_2}{2}x\right)\cos\left(\frac{k_2 - k_1}{2}x\right)$$

in the domain $[-3\pi, 3\pi]$. We set $k_1 = \omega_1 = 6$, $k_2 = 8$, and $\omega_2 = 12$. The exact group and phase velocities were $V_{g,\,exact} = 3$ and $V_{p,\,exact} = 9/7$. The initial distribution and its envelope derived with a Hilbert transform are shown in Fig. 10. Here, $N_x = 120$, $T = 1$, and $\Delta t = 5 \times 10^{-4}$.

The corresponding envelopes, which contain information about the group velocity, were derived by Hilbert transform [13], as shown in Fig. 11. By convention, the envelopes were drawn after taking the absolute value. The details to derive envelopes are shown in the Appendix. For the purpose of further comparison, the result of linear counterpart of WENO7-JS, UPW7, which has lower dissipation, is also given in Fig. 11.

Figure 11 shows that UPW7 yields a result closest to the exact solution, which is due to its relatively smallest spectrum error such as low dissipation. Besides, UPW5 yields an envelope such that the numerical group velocity is closest to the theoretical one of the remaining three schemes, followed by WENO5-M and then WENO5-JS. The amplitudes of the envelope show that UPW5 had the least dissipation,
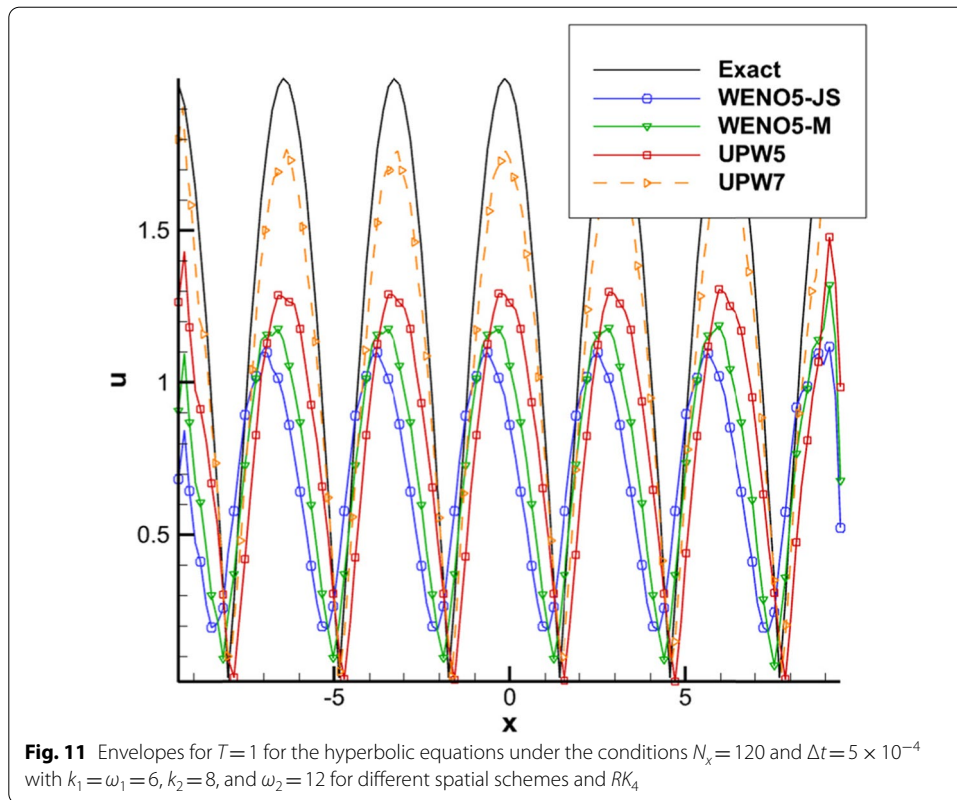
Fig. 10 Distributions of initial combination wave and its envelope for $k_1 = \omega_1 = 6$, $k_2 = 8$, and $\omega_2 = 12$

followed by WENO5-M and then WENO5-JS. Recall that from Fig. 3, the area of GVP given by QL-GRP was in the order: UPW5 > WENO5-M > WENO5-JS. Therefore, the results for QL-GRP agree with the numerical results, which verifies its validity.

6 Conclusions

Because GRP [5] cannot be used for a group velocity analysis of a nonlinear scheme, QL-GRP was proposed by combining ADR with GRP. Moreover, a detailed derivation and implementation of QL-GRP were provided for high-order Runge–Kutta schemes. The conclusions are as follows:

1. Since QL-GRP can analyze the GVP for nonlinear schemes, it can distinguish between the group velocity of different schemes. When the spatial scheme is linear, QL-GRP degenerates to GRP.
2. The group velocities of typical schemes were derived numerically and the comparison confirmed the rationality of QL-GRP.
3. If the reduced frequency is small, the group velocity given by QL-GRP is accurate. Moreover, its predictions are reasonable and meaningful at medium reduced frequency. Although QL-GRP cannot accurately predict the GVP at high reduced

Xu *et al. Advances in Aerodynamics*   (2022) 4:14

Page 21 of 23

Fig. 11 Envelopes for $T = 1$ for the hyperbolic equations under the conditions $N_x = 120$ and $\Delta t = 5 \times 10^{-4}$ with $k_1 = \omega_1 = 6$, $k_2 = 8$, and $\omega_2 = 12$ for different spatial schemes and RK_4

frequency, it can provide a reference in an analysis of the group velocity of nonlinear schemes.

4. Hyperbolic equations were devised for combination waves with different group and phase velocities. These enabled numerical investigations. Through two numerical examples, the validity of QL-GRP was verified qualitatively and quantitatively.

As indicated in this study, distinct GVP regions exist among schemes with different performances regarding GRP, hence such information would be used to define the (free) parameters in optimized schemes and schemes with additional control parameters. Besides, it is known the multiple waves would yield nonlinear interaction through nonlinear schemes, which has drawn the attention in nonlinear spectrum analysis in [14]. It is natural to extend the current analysis to one that considers the interaction of multiple waves. Due to the limitation of space, such a topic will be discussed in other investigations.

Appendix

The main codes on deriving the envelopes by MATLAB are as follows:

```
U = abs(hilbert(a)); % "a" represents the numerical value.
plot(b, U); % "b" represents the x-coordinate, "U" represents the envelope.
```

(a) t=0

(b) t=3

Fig. 12 Envelope of the distribution $u = 2\cos(3x - 5t)\cos(x - 3t)$ at different moments
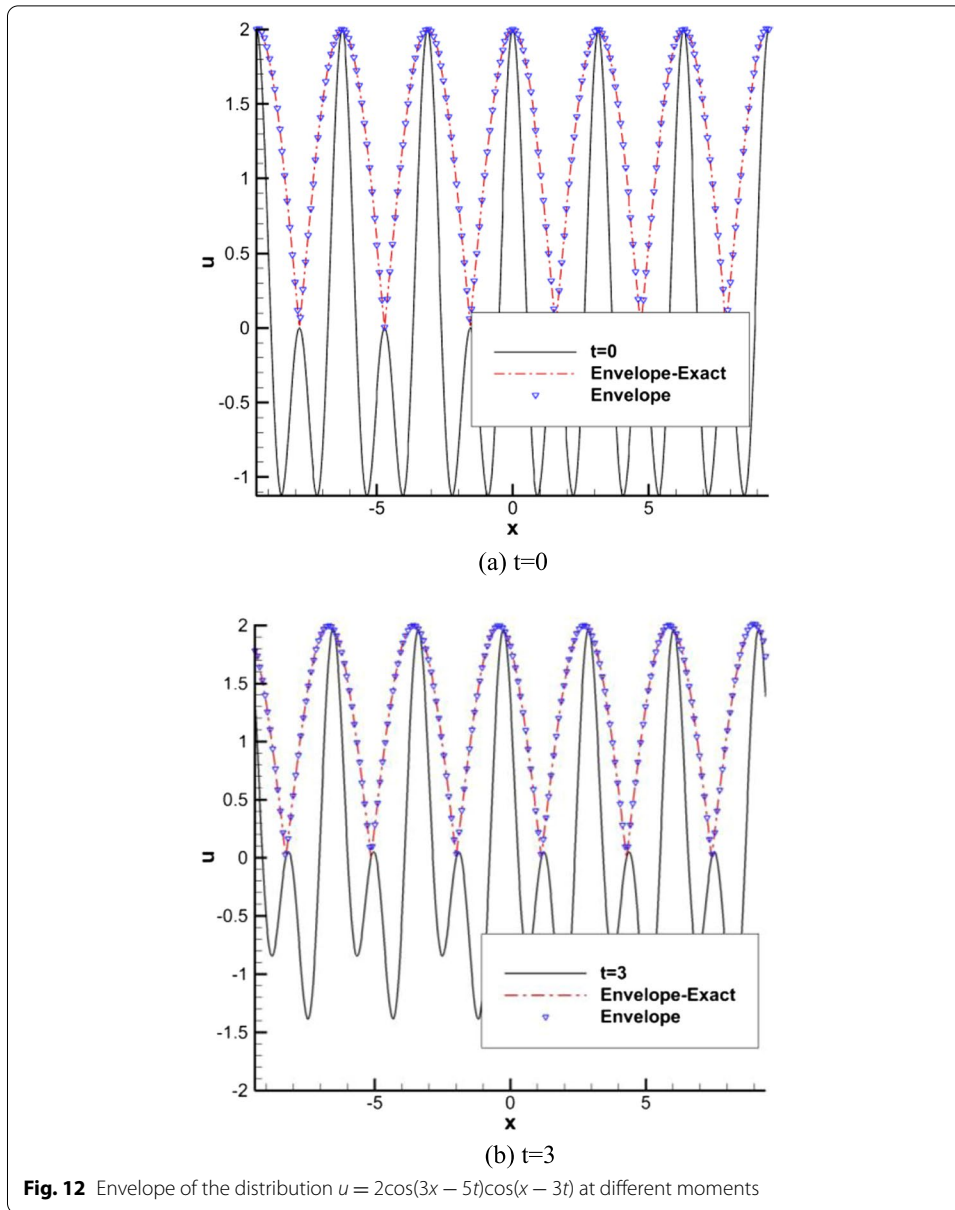
Taking the distribution $u = 2\cos(3x - 5t)\cos(x - 3t)$ as an example, the derived envelopes at different moments are depicted in Fig. 12, which shows that the numerical envelope obtained by the codes is the same as the exact one.

Declarations

Competing interests

References

1. Tam CKW, Webb JC (1993) Dispersion-relation-preserving finite difference schemes for computational acoustics. J Comput Phys 107:262–281
2. Pirozzoli S (2006) On the spectral properties of shock-capturing schemes. J Comput Phys 219:489–497
3. Mao ML, Yan ZG, Liu HY et al (2015) Study of quasi-linear spectral analysis method of high-order weighted nonlinear schemes. Acta Aerodyn Sin 33(1):1–9
4. Sengupta TK, Sircar SK, Dipankar A (2006) High accuracy schemes for DNS and acoustics. J Sci Comput 26:151–193
5. De AK, Eswaran V (2006) Analysis of a new high resolution upwind compact scheme. J Comput Phys 218:398–416
6. Sengupta TK, Ganeriwal G, De S (2003) Analysis of central and upwind compact schemes. J Comput Phys 192:677–694
7. Jiang GS, Shu CW (1996) Efficient implementation of weighted ENO schemes. J Comput Phys 126:202–228
8. Lele SK (1992) Compact finite difference schemes with spectral-like resolution. J Comput Phys 103:16–42
9. Henrick AK, Aslam TD, Powers JM (2005) Mapped weighted essentially non-oscillatory schemes: achieving optimal order near critical points. J Comput Phys 207:542–567
10. Li X-L, Leng Y, He Z-W (2013) Optimized sixth-order monotonicity-preserving scheme by nonlinear spectral analysis. Int J Numer Methods Fluids 73:560–577
11. Li Q, Guo Q-L, Zhang H-X (2013) Analyses of the dispersion overshoot and inverse dissipation of the high-order finite difference scheme. Adv Appl Math Mech 5:809–824
12. Vichnevetsky R, Bowles JB (1982) Fourier analysis of numerical approximations of hyperbolic equations. SIAM, Philadelphia
13. Dong D, Li XC (2018) On a hybrid of bilinear Hilbert transform and paraproduct. Acta Math Sin 34:29–41
14. Fauconnier D, Dick E (2011) On the spectral and conservation properties of nonlinear discretization operators. J Comput Phys 230:4488–4518

Publisher's Note